ARMA 10-114

Strength Anisotropy of Mudstones and Shales

Ewy, R. T. and Bovberg, C. A.
Chevron Energy Technology Co., San Ramon / Richmond, CA, USA
Stankovic, R. J.
RSTD Co., Park City, UT, USA

This paper was prepared for presentation at the 44th US Rock Mechanics Symposium and 5th U.S.-Canada Rock Mechanics Symposium, held in Salt Lake City, UT June 27–30, 2010.

ABSTRACT: Compressive strength anisotropy of six different claystones was measured, using confined triaxial compression tests. Samples were oriented with the bedding perpendicular to the axial stress, and with the bedding at an acute angle to the axial stress in order to cause slip on bedding. Measured strengths were resolved into values of normal stress and shear stress, and these were fit with linear regression to determine values of cohesion and friction angle. Slip on bedding was found to reduce the cohesion by 10% to 70%, and reduce the friction angle by 7% to 17%, with higher reduction generally observed for the lower-porosity rocks. Loading parallel to bedding resulted in the same strength as loading perpendicular to bedding.

1. INTRODUCTION

Shales make up the vast majority of formations that must be drilled through to reach oil and gas reservoirs. In some cases, especially with recent shale gas developments, the shales themselves are the reservoir. Shale mechanical behavior impacts drilling and wellbore stability. It also impacts casing damage that can occur after a field is on production. Many instances of shale bedding-related instabilities, caused by strength anisotropy, have been reported in the oilfield literature. Highly-inclined wellbores, drilled nearly parallel to bedding, can be very unstable due to bedding-related failure. Shale mechanical behavior is also important in mining, especially coal mining, and in civil engineering. In these areas as well, shale strength anisotropy can have a large impact.

The goal of this study was to quantify strength anisotropy for a cross-section of different shales. The shales were selected to represent a variety of different in-situ compaction states, ranging from low-porosity shales to those with fairly high porosity. All samples are clay-rich, containing 65% or greater clay. Preserved downhole shale cores were used for all samples.

The methodology employed was to quantify cohesion and friction angle for failure not influenced by bedding, and compare this to the cohesion and friction angle measured directly from slip on bedding. This was accomplished using confined triaxial compression tests at different levels of confining stress, and using two different sample orientations relative to bedding. For one orientation, axial loading was perpendicular to bedding, while for the other orientation axial loading was at an acute angle to bedding. For one of the shales, a third orientation was used with axial loading parallel to bedding.

2. SAMPLE DESCRIPTION

Six different claystones (referred to as ‘shales’ in this paper) were used for this study. According to most rock classification schemes, claystone covers all clay-rich rocks with or without fissility, whereas the term shale is reserved for claystones that exhibit fissility. All six of our studied rocks are referred to loosely as ‘shales’ even though most of them are not very fissile. Claystones that do not exhibit fissility are usually classified as mudstones.

Preserved oilwell cores were used for this study. These shale cores come from different locations around the world and from depths ranging from 5000 to 13000 feet. Increasing burial depth causes greater compaction. Therefore, these shales represent a variety of compaction (consolidation) states.

Key parameters for these shales are listed in Table 1. The porosity is a reflection of the compaction state. As evident from the table, all the shales are clay-rich. All

but one have a clay content of approximately 75%, while shale B is closer to 65%.

Table 1. Porosity, clay content and CEC of the studied shales

Shale	Porosity*	Total Clay (wt%)**	CEC (meq/100g)
A	26.0%	75	20
B	17.8%	64	29
C	14.2%	76	25
D	15.3%	75	24
E	13.9%	77	18
F	8.5%	75	35

*measured via high-pressure mercury injection
**from x-ray diffraction

The Cation Exchange Capacity (CEC) listed in Table 1 is a proxy for the total amount of smectite in each shale. Smectite contributes 6 to 8 times more CEC than does illite, and other clays such as kaolinite and chlorite have negligible CEC. Therefore, high CEC indicates a high fraction of smectite in the shale. A high ratio of CEC to total clay indicates that the clay fraction is smectite-rich.

All shale samples were cut from fully-preserved shale cores. Each shale core was cut in the field using non-aqueous (e.g. oil or synthetic base) fluid. The cores were then sealed and kept fully-preserved. Samples of size 19mm (0.75 in.) diameter by 38mm (1.5 in.) length were cut using decane as the lubricant, and the samples were also kept wet with decane during the end-grinding process. Following this, the samples were either re-immersed in decane or placed in vacuum desiccators of controlled relative humidity. Thus, the water content was tightly controlled during all stages of sample preparation, and was also kept close to the native water content of each shale.

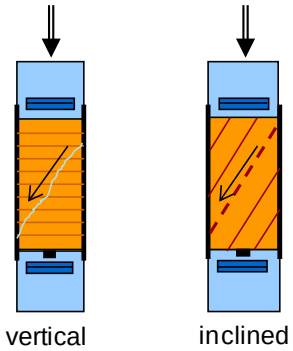

Fig. 1. Bedding vs. sample axis for two orientations.

From each shale, sets of samples were cut in two different orientations. The first set was cut with the sample axes perpendicular to bedding. These are referred to as 'vertical' samples. The second set was cut at an angle to bedding, with the bedding aligned roughly 30°-40° relative to the sample axis (the normal-to-bedding aligned 50°-60° relative to the sample axis). These are referred to as 'inclined' samples. These two orientations are illustrated in Figure 1.

3. METHODOLOGY

For each shale, the triaxial compression failure envelope was first determined for the vertical sample set. Strengths were measured under different conditions of effective confining stress, using a different confining stress for each sample. For the vertical samples, the failure does not involve the bedding planes, as the shear fracture cuts across bedding at a steep angle (see Figure 1).

The same type of tests were then performed using the inclined samples. Due to the chosen angle of the bedding planes, failure in these samples occurred by shear slip along the bedding planes. By testing inclined samples at different values of effective confining stress, it is possible to directly determine both the cohesion and friction angle of the bedding planes. This can then be compared to the failure envelope determined for the vertical samples.

3.1. Test Apparatus and Method

Because shales have extremely low permeabilities, generally in the range 0.1 to 10 nanodarcy (10^{-22} to 10^{-20} m^2), it is not feasible to conduct drained triaxial compression tests. All the tests conducted for this study were undrained, with continuous measurement of sample pore pressure.

The apparatus used for the undrained triaxial compression tests is illustrated in Figure 2, and a full description can be found in [1]. The samples were first placed under confining stress and allowed to consolidate under an undrained condition. The native pore fluid in the sample would give rise to a pore pressure. The amount of pore pressure cannot be set exactly, but it can be generally controlled by equilibrating the sample to a designated relative humidity prior to the test.

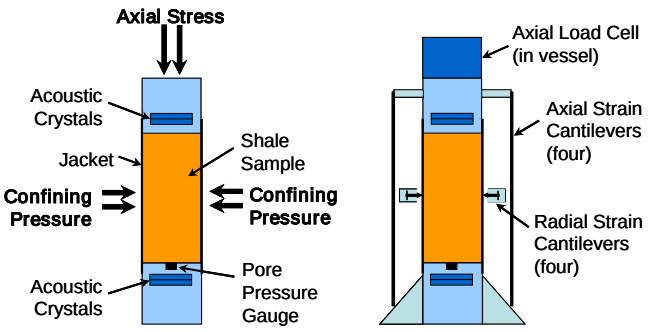

Fig. 2. Schematic of shale triaxial setup.

After full equilibrium was obtained under hydrostatic confining stress, deviatoric loading was applied. Axial strain rates of 5E-08 to 2E-07 1/sec were used. The correct strain rate was determined using the method presented in [2]. The strain rate must be slow enough to allow full pore pressure equilibrium throughout the sample during the test. Even undrained tests require extremely slow loading rates and small samples, due to the extremely low values of shale permeability.

An example pressure vs. time plot is shown in Figure 3. This illustrates the initial hydrostatic loading phase (waiting for pore pressure equilibrium), followed by the deviatoric loading phase. The pore pressure is seen to track the deviator load quite well, which is an indication that pore pressure is at equilibrium throughout the sample during this loading phase.

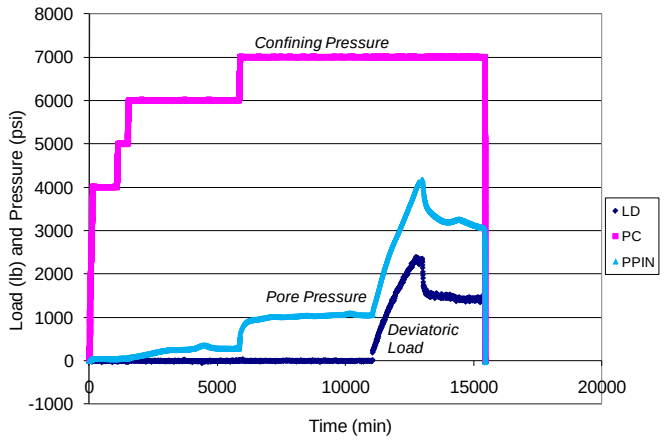

Fig. 3. Example stress/pressure vs. time plot for Shale E, consolidated undrained triaxial compression test.

Certain samples from shales B and E were tested using an alternate bottom end-cap arrangement that includes a pore line, with the pore line valve closed. The fluid volume between the sample and the valve is approximately 0.3 cc, which is small enough to ensure that the samples were very close to an undrained condition during these tests.

3.2. Data Reduction

When each sample reaches a compressive (shear) failure condition, there are measured values for deviatoric stress, confining stress, and pore pressure. These are converted to values of effective confining stress and effective axial stress (at failure) for each sample.

For the vertical sample sets from each shale, a linear least-squares regression was fit to these effective confining stress vs. effective axial stress data points, as illustrated in Figure 4. The intercept of this best-fit line is the UCS-intercept, and the slope is related to the friction angle. These can be converted to equivalent values of cohesion (c) and friction angle (ϕ) using the following two equations:

$$\phi = \sin^{-1}\left[\frac{q-1}{q+1}\right] \qquad (1)$$

$$c = \frac{C_0}{2\tan\left(45+\frac{\phi}{2}\right)} \qquad (2)$$

where q is the slope of the best-fit line as in Figure 4, and *Co* is the intercept of the best-fit line.

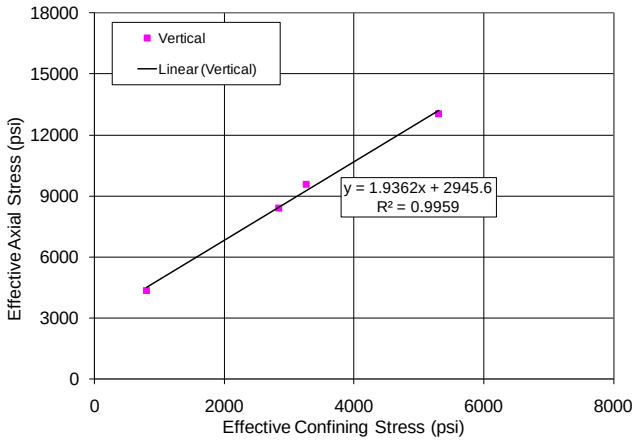

Fig. 4. Peak strength (effective axial stress) vs. effective confining stress for Shale E vertical samples.

For the inclined samples the data were processed differently, in order to directly obtain cohesion and friction angle of the bedding. For each individual sample the inclination of the shear plane was carefully measured. Using this inclination angle, the values of effective confining stress and effective axial stress (at failure) were converted to values of shear stress (τ) and effective normal stress (σ_n). This was accomplished using the following two equations:

$$\sigma_n = \sigma_1 \cos^2(\gamma) + \sigma_3 \sin^2(\gamma) \qquad (3)$$

$$\tau = (\sigma_1 - \sigma_3)\sin(2\gamma) \qquad (4)$$

where σ_1 and σ_3 are the effective axial stress and effective confining stress at failure, respectively, and γ is the angle between the bedding-plane normal and the axial stress.

For each shale, the set of inclined samples therefore provides a collection of shear stress vs. effective normal stress values. A linear least-squares regression was fit to these values. This directly determines the best-fit value for the cohesion and friction angle of the bedding plane, for that shale.

In order to visually compare the bedding-strength values to the vertical sample results, the values of effective confining stress and effective axial stress from the vertical samples were also converted to equivalent values of shear stress and effective normal stress. However, in this case the friction angle for use in Eqns. 3 and 4 was taken as the angle of internal friction given by Eqn. 1.

In order to compare results from all six shales on the same basis, for each shale all values of shear stress and effective normal stress were then divided by the vertical sample best-fit cohesion from Eqn. 2. This normalization was performed for both the vertical and the inclined results.

4. RESULTS

The results from Shale A are plotted in Figure 5. The line that represents the strength of the vertical samples (as determined by equations 1 and 2) is shown. Because it is normalized by the cohesion from Eqn. 2, its intercept is exactly equal to 1.0. The measured strengths of the vertical samples, after conversion to equivalent values of shear stress and effective normal stress (as described above in Data Reduction) are also shown.

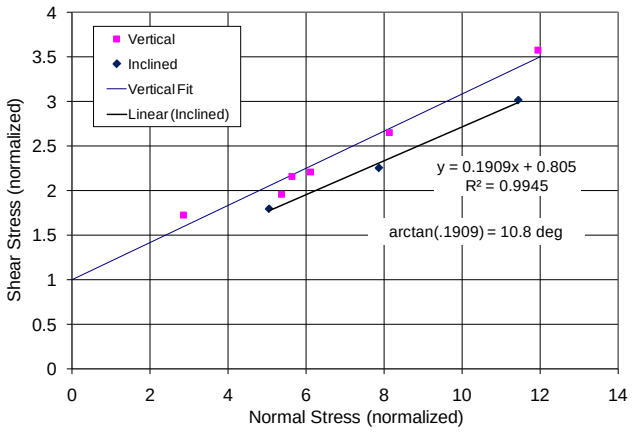

Fig. 5. Shear stress vs. effective normal stress for vertical and inclined samples, Shale A.

The values of shear stress and effective normal stress corresponding to shear on bedding, from the inclined samples, are also shown in Figure 5 and are fit with a linear least-squares regression. Since these values are normalized by the vertical sample cohesion, the intercept of this line directly indicates the amount of cohesion reduction. Since the intercept is ~0.80, the bedding-plane cohesion is ~20% lower than the cohesion for shear that is not affected by bedding.

The slope of the regression line in Figure 5 directly gives the friction coefficient of the bedding planes. As noted in the figure, the value of 0.19 converts to a friction angle of 10.8°. It is seen that this is only slightly less than the slope of the strength line for the vertical samples. Thus, strength anisotropy for this shale is mostly manifested as a reduction in cohesion rather than a reduction in friction angle.

The results from Shale B are plotted in Figure 6. Just as for Shale A, all data values have been normalized by the best-fit cohesion for the vertical samples, as determined from Eqn. 2. Very similar to shale A, the cohesion of the bedding planes is ~20% (19% to be precise) lower than the cohesion for shear that does not involve bedding. The bedding friction angle for Shale B is greater than that of Shale A (13.1° vs. 10.8°), but similar to Shale A it is only slightly less than that for the vertical samples. So, again, for Shale B the strength anisotropy is manifested mainly as a reduction in cohesion rather than a reduction in friction angle.

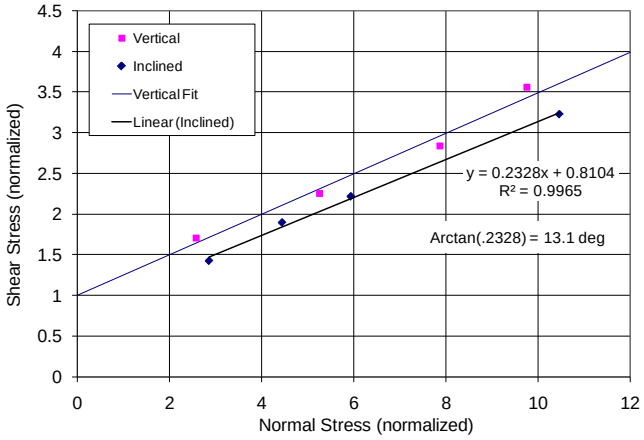

Fig. 6. Shear stress vs. effective normal stress for vertical and inclined samples, Shale B.

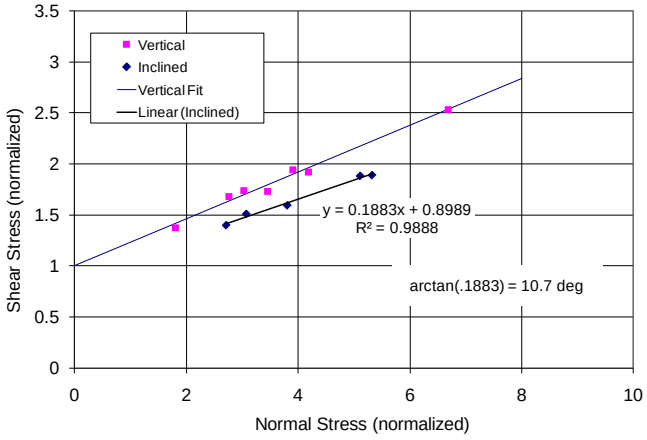

Fig. 7. Shear stress vs. effective normal stress for vertical and inclined samples, Shale C.

Figure 7 shows the results for Shale C. In this case the bedding-plane cohesion is only ~10% lower than the

cohesion for shear that is not affected by bedding. However, it is seen that the slope of the bedding-shear line is noticeably lower than the slope of the vertical sample line. For Shale C, strength anisotropy appears as both a reduction in cohesion and a reduction in friction angle. However, the overall level of strength anisotropy is fairly small for this shale. Exact values of cohesion reduction and friction angle reduction for all six shales are documented later in this section.

Results for Shales D and E are shown in Figures 8 and 9, respectively. For both of these shales, strength anisotropy is significant. The bedding-plane cohesion for these shales is 45%-50% less than the cohesion for shear that does not involve bedding. The bedding-plane friction angle is also somewhat less than the vertical-sample friction angle, more so for Shale E than for Shale D. Overall, however, the strength anisotropy is mostly seen as a reduction in cohesion.

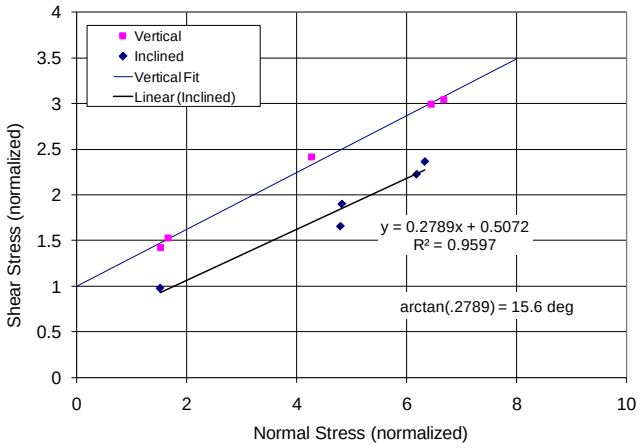

Fig. 8. Shear stress vs. effective normal stress for vertical and inclined samples, Shale D.

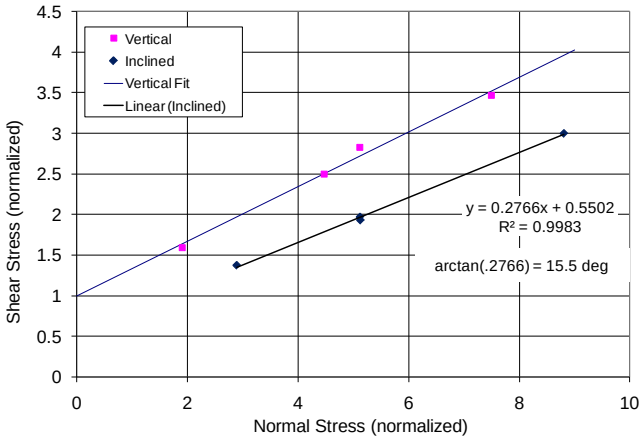

Fig. 9. Shear stress vs. effective normal stress for vertical and inclined samples, Shale E.

Results for Shale F are shown in Figure 10. For this shale, the bedding-plane results span a very short range of normal stress values, so short that it is not possible to obtain a meaningful linear least-squares regression. The regression indicates that the bedding-plane friction angle is greater than that of the vertical samples, which is highly unlikely. However, the inclined samples provide good measurements of residual (post-slip) bedding strength as well as some measurements of bedding slip on pre-fractured samples. Since these data points should correspond to zero cohesion, a fit is obtained to these data which is forced through the origin (see Figure 10). The slope of this line provides an approximate value for the bedding-plane friction angle, which is ~9°.

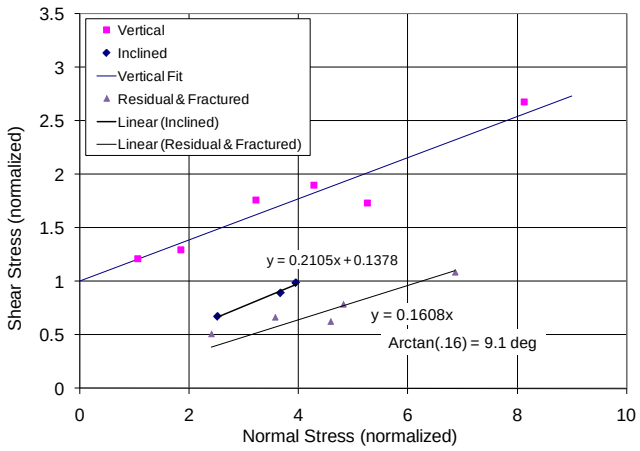

Fig. 10. Shear stress vs. effective normal stress for vertical and inclined samples, Shale F.

Using the value of 9°, each of the three inclined strength data points can be extrapolated back to zero normal stress. Doing this, one obtains normalized cohesion values of 0.27 to 0.36, with an average of 0.32. In other words, this is equivalent to fitting a line through the three data points with a slope of 0.16 and an intercept of 0.32.

An alternate method for evaluating the bedding-plane strength for Shale F is to assume that the bedding-plane friction angle is exactly the same as the friction angle from the vertical samples, which is an already-low value of 10.9°. In this case, extrapolating the three bedding data points to zero normal stress gives an average normalized cohesion of 0.2.

Thus, the bedding-plane cohesion for Shale F is ~70% (and perhaps up to 80%) lower than the cohesion for shear that does not involve bedding. In either case, the cohesion reduction is large and is the greatest observed out of all six shales tested.

The measured values of cohesion ratio and friction angle ratio are summarized in Table 2. The cohesion ratios range from 0.32 to 0.90, and the friction angle ratios range from 0.83 to 0.93. Thus, as observed visually from Figures 5 through 10, there is more variation of

cohesion ratio for the six shales than there is for friction angle ratio. Cohesion ratio is defined as the bedding-plane cohesion divided by the best-fit cohesion for the vertical samples (from Eqn. 2). Friction angle ratio is defined as the bedding-plane friction angle divided by the best-fit friction angle for the vertical samples (from Eqn. 1).

Table 2. Bedding-plane cohesion and friction angles, relative to the values obtained with no bedding slip (vertical samples).

Shale	Cohesion Ratio	Friction Angle Ratio
A	0.81	0.91
B	0.81	0.93
C	0.90	0.83
D	0.51	0.90
E	0.55	0.83
F	0.32*	0.83*

*alternate fit is possible – see text

For Shale E, triaxial compression tests were also performed on a set of samples cut with their axes parallel to bedding ('horizontal' samples). Figure 11 shows the measured strengths of these samples, as a function of effective confining stress. Also included in this plot are the strengths of the vertical samples (from Figure 4) and the strengths of the inclined samples. For Shale E, all the inclined samples had bedding inclined ~30° to the sample axis; because of this constant bedding orientation, it is meaningful to plot the results as major stress vs. minor stress.

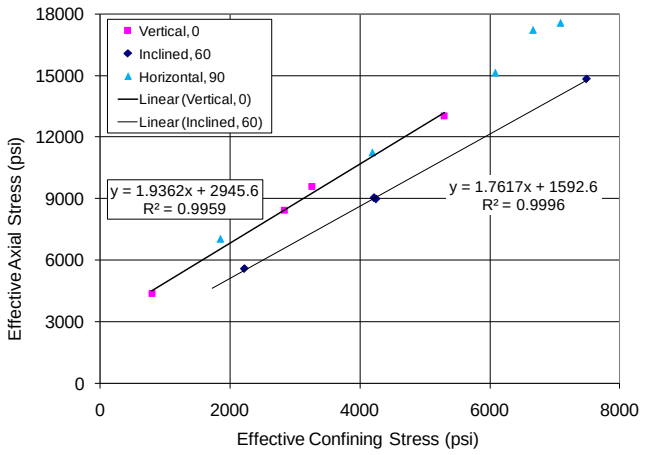

Fig. 11. Effective axial stress (at failure) vs. effective confining stress for vertical, horizontal and inclined samples, Shale E.

The strengths of the horizontal samples lie slightly above the best-fit line to the vertical samples, and a fit to just the horizontal samples would have a slightly greater friction angle. But given the data scatter, it can be concluded that the horizontal samples have about the same strength as the vertical samples. The inclined samples clearly are much weaker, due to the shear slip which occurs along bedding. For both the vertical and horizontal samples, the shear fracture cuts across bedding and does not appear to be influenced by the bedding shear strength.

5. DISCUSSION

The results from shale E confirm one of the predictions from the 'single plane-of-weakness' theory. This theory, which is applicable to multiple parallel planes of weakness (bedding planes), predicts that vertical and horizontal samples will have the same strength, but that inclined samples will have lower strength. The predicted strength, for any single level of confining stress, is shown in Figure 12 as a function of bedding angle relative to the sample axis [3].

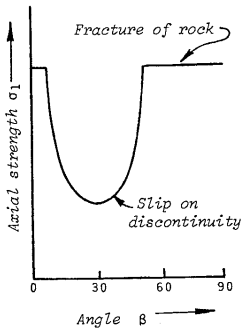

Fig. 12. Predicted strength vs. angle of bedding relative to maximum stress, from plane-of-weakness theory [3].

The equation describing the curve in Figure 12, and the supporting derivation, can be found in several rock mechanics reference books [3, 4, 5]. Failure on the curved part of the line, rather than on the flat, horizontal part of the line, occurs when it is easier to slip on bedding than it is to create a shear fracture that cuts across bedding. The extent and shape of the curved portion of the line depend on the bedding-plane cohesion and friction angle, relative to the cohesion and friction angle for shear that cuts across bedding.

The position of the curve minimum is not always at 30° as shown in Figure 12. The minimum strength occurs for bedding inclined relative to the sample axis at an angle of (45° - ϕ_b/2), where ϕ_b is the friction angle of the bedding planes. For the shales we have tested, the bedding friction angles are in the range 9° to 16°. This suggests that minimum strength would occur for bedding inclined at 37° – 40° to the sample axis, for these shales.

The single-plane-of-weakness theory may not exactly describe the failure of shales for all possible bedding-plane inclinations. Example lab data from phyllites,

slates and shales are shown in Figure 13 [5]. Additional data can be found in [3]. It is seen that the 'corners' of the curve, where it should theoretically join the flat line (see Figure 12), are rounded off. Alternative theories and empirical methods that account for this can be found in [3, 4, 5, 7]. The shale data in Figure 13 and in the quoted references were likely obtained using standard triaxial testing on 'dry' samples; therefore, the results might not represent in-situ failure, depending on the shale clay content and water content.

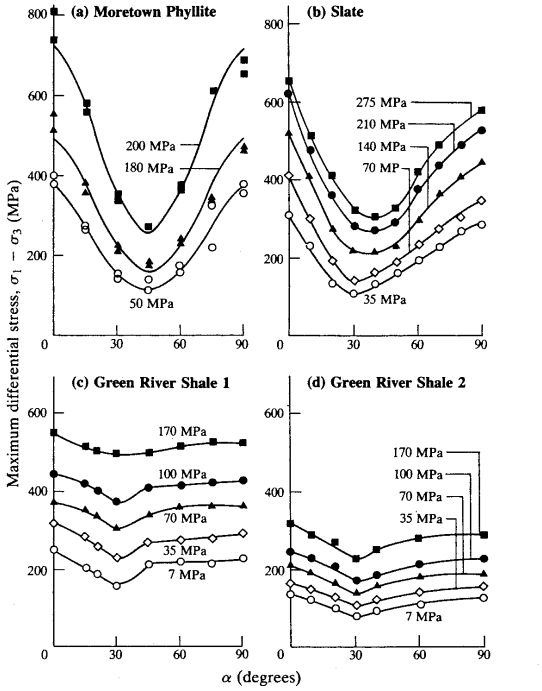

Fig. 13. Measured strengths vs. bedding inclination, at different levels of confining stress [5, from 6, 7].

For the curves in Figure 13, the amount of strength reduction with changing inclination represents the reduction in cohesion, while the spacing between the multiple curves represents the friction angle for any particular bedding orientation. If the curve spacing changes with changing bedding orientation then this indicates that the bedding-plane friction angle is different than the friction angle for shear that cuts across bedding. The data in Figure 13 are compatible with our findings of a reduction in cohesion, which can be either small or large, along with a slight reduction in friction angle.

There is a rough relationship between our measured cohesion ratios (Table 2) and the compaction state of our shales, as represented by porosity. This is shown in Figure 14. Other than Shale C, which is an outlier, there is general trend of decreasing cohesion ratio with decreasing shale porosity (increasing compaction). Shale B also lies above the general trend, which may be due to its slightly lower clay content (~65% compared to ~75% for the other shales). While Figure 14 suggests that clay content may affect the cohesion ratio, tests on additional shales with other clay contents would be needed in order to confirm this. At this time we have no explanation for the high cohesion ratio observed on Shale C.

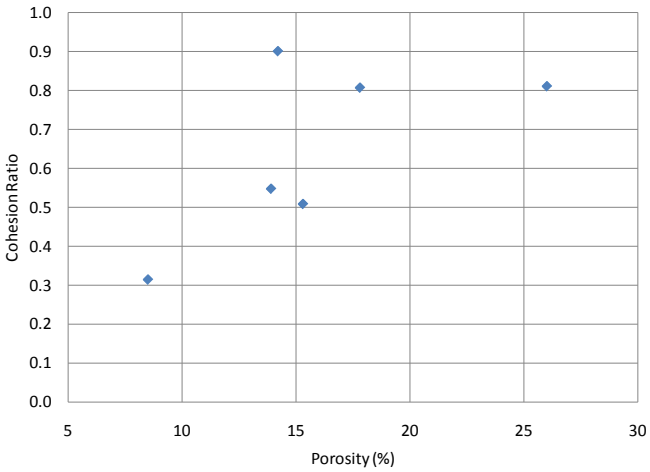

Fig. 14. Cohesion ratio generally decreases with decreasing shale porosity (data from Tables 1 and 2).

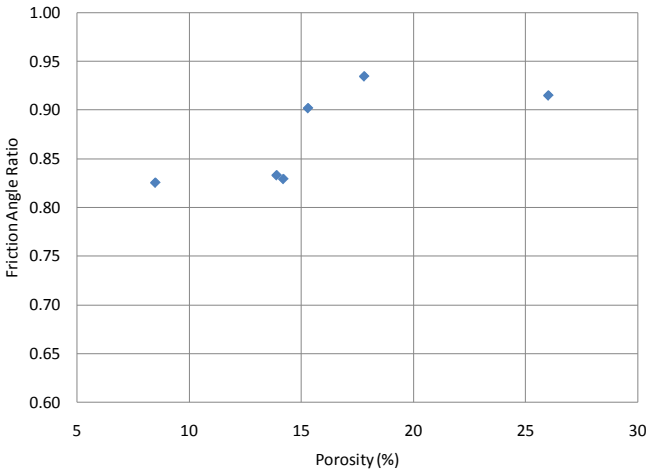

Fig. 15. Friction angle ratio somewhat decreases with decreasing shale porosity (data from Tables 1 and 2).

Friction angle ratio is plotted vs. shale porosity in Figure 15. There is a loose trend of decreasing friction angle ratio with decreasing porosity. Shale B lies above the general trend, again possibly due to its lower clay content. Shale C lies within the trend on this plot. However, if the fit to Shale C bedding cohesion and friction angle were slightly steeper, it would have a slightly higher friction angle ratio (which would still be within the general trend in Figure 15) but would also have a lower cohesion ratio, perhaps closer to the general trend in Figure 14. Thus, Shale C might be an outlier simply due to the vagaries of laboratory testing

and the manner in which the least-squares fits happened to turn out.

Qualitatively, the measured strength anisotropy correlates with the observed fissility of these shales. The more highly compacted shales generally were more troublesome during sample preparation, with samples more likely to part along the bedding planes. Shale F was by far the most fissile of all the shales tested, with bedding-plane parting very common. This correlates with the measured high degree of strength anisotropy on this shale.

One might expect that higher smectite content would increase the strength anisotropy, resulting in a lower cohesion ratio and a lower friction angle ratio. Since whole-rock CEC is a proxy for the total amount of smectite in the shale, cohesion ratio and friction angle ratio are plotted against CEC in Figures 16 and 17. From these figures, there does not appear to be any consistent influence of CEC on either cohesion ratio or friction angle ratio.

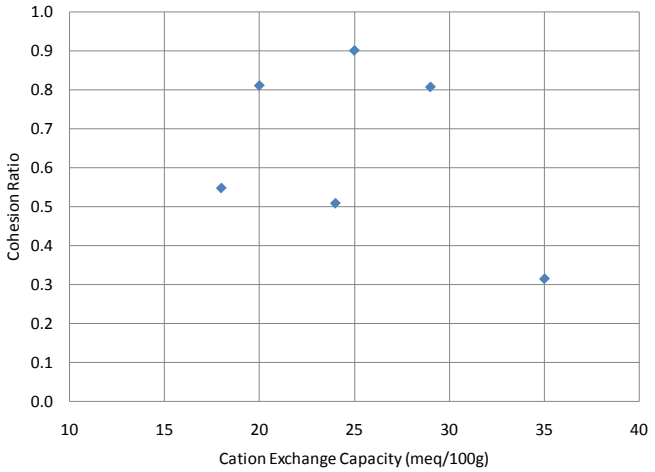

Fig. 16. Cohesion ratio does not correlate with shale CEC.

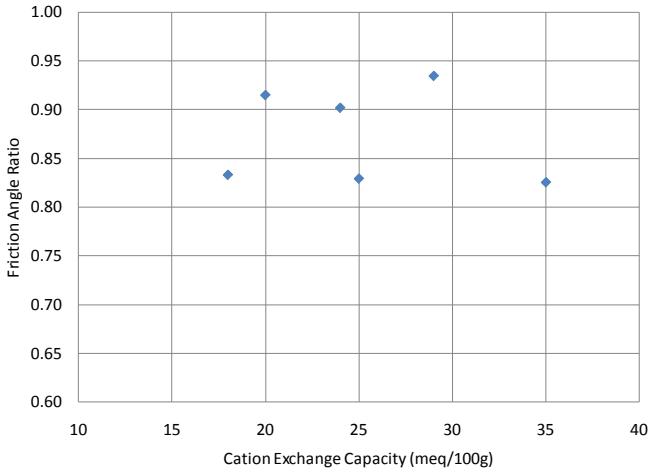

Fig. 17. Friction angle ratio does not correlate with shale CEC.

6. CONCLUSIONS

Claystones ('shales') can exhibit varying degrees of strength anisotropy, as demonstrated by this study. For some samples the bedding-plane cohesion was only 10% to 20% less than the cohesion for shear that does not involve slip on bedding. For others it was ~50% less, and in one case it was ~70% less. Friction angle was found to be less affected. In all cases the bedding-plane friction angle was slightly less than the friction angle for shear that does not involve slip on bedding, with the reduction being in the range 7% to 17%.

Greater in-situ compaction seems to correlate with greater strength anisotropy, at least for most of the shales in this dataset. The greatest reductions in cohesion, and friction angle, were observed on the lower-porosity shales. The lower-porosity shales also tended to be more fissile when preparing samples. Qualitatively, this correlates with the measured degree of strength anisotropy. The amount of smectite in the shale, as represented by cation exchange capacity, was found to not correlate with strength anisotropy.

For one shale, loading was performed parallel to bedding as well as perpendicular to bedding. Strength was found to be essentially the same for both these orientations, suggesting that the strength of the bedding planes does not affect failure for either of these loading orientations.

ACKNOWLEDGEMENTS

Many thanks to J. Mercado and M. Shalz for assisting with sample preparation and handling. Mineralogical and petrophysical data were provided by D. McCarty and B. McCollom. Thanks also to Chevron management for support of these studies and for permission to publish. This work was performed as part of a Shale Characterization strategic research project.

REFERENCES

1. Ewy, R.T., R.J. Stankovich, and C.A. Bovberg 2003. Mechanical behavior of some clays and shales from 200m to 3800m depth. In *Proceedings 'Soil Rock America' 39th U.S. Rock Mechanics Symp. / 12th Panamerican Conf. on Soil Mech. & Geotech. Eng., Cambridge, MA, 22-26 June 2003*, eds. P. Culligan, H. Einstein and A. Whittle, 445-452 (paper 570). Essen: Verlag Gluckauf.

2. Ewy, R.T. 2001. Behavior of a reactive shale from 12000 feet depth. In *Proceedings 38th U.S. Rock Mechanics Symp. 'DC Rocks', Washington DC, 7-10 July 2001*, eds. D. Elsworth, J. Tinucci and K. Heasley, 77-84. Lisse: Balkema.

3. Hoek, E. and E.T. Brown. 1982. *Underground excavations in rock*. 2nd ed. London: Institution of Mining and Metallurgy.

4. Jaeger, J.C.. and N.G.W. Cook. 1979. *Fundamentals of rock mechanics*. 3rd ed. London: Chapman and Hall.

5. Brady, B.H.G. and E.T. Brown. 1985. *Rock mechanics for underground mining*. 1st ed. London: George Allen & Unwin.

6. Donath, F.A. 1972. Effects of cohesion and granularity on deformational behavior of anisotropic rock. In *Studies in mineralogy and Precambrian geology*, ed. B.R. Doe and D.K. Smith, 95–128, Geol. Soc. America Memoir 135.

7. McLamore, R. and K.E. Gray. 1967. The mechanical behavior of anisotropic sedimentary rocks. *J. Engng. For Industry, Trans Am. Soc. Mech. Engrs Ser. B.* 89: 62-73.